Predictability of the Madden–Julian Oscillation in the Intraseasonal Variability Hindcast Experiment (ISVHE)*

J. M. NEENA

Joint Institute for Regional Earth System Science and Engineering, University of California, Los Angeles, Los Angeles, California

JUNE YI LEE

International Pacific Research Center, University of Hawai'i at Mānoa, Honolulu, Hawaii, and Institute of Environmental Studies, Pusan National University, Busan, South Korea

DUANE WALISER

Joint Institute for Regional Earth System Science and Engineering, University of California, Los Angeles, Los Angeles, and Jet Propulsion Laboratory, California Institute of Technology, Pasadena, California

BIN WANG

International Pacific Research Center, University of Hawai'i at Mānoa, Honolulu, Hawaii

XIANAN JIANG

Joint Institute for Regional Earth System Science and Engineering, University of California, Los Angeles, Los Angeles, California

(Manuscript received 16 October 2013, in final form 23 February 2014)

ABSTRACT

The Madden–Julian oscillation (MJO) represents a primary source of predictability on the intraseasonal time scales and its influence extends from seasonal variations to weather and extreme events. While the last decade has witnessed marked improvement in dynamical MJO prediction, an updated estimate of MJO predictability from a contemporary suite of dynamic models, in conjunction with an estimate of their corresponding prediction skill, is crucial for guiding future research and development priorities. In this study, the predictability of the boreal winter MJO is revisited based on the Intraseasonal Variability Hindcast Experiment (ISVHE), a set of dedicated extended-range hindcasts from eight different coupled models. Two estimates of MJO predictability are made, based on single-member and ensemble-mean hindcasts, giving values of 20–30 days and 35–45 days, respectively. Exploring the dependence of predictability on the phase of MJO during hindcast initiation reveals a slightly higher predictability for hindcasts initiated from MJO phases 2, 3, 6, or 7 in three of the models with higher prediction skill. The estimated predictability of MJO initiated in phases 2 and 3 (i.e., convection in Indian Ocean with subsequent propagation across Maritime Continent) being equal to or higher than other MJO phases implies that the so-called Maritime Continent prediction barrier may not actually be an intrinsic predictability limitation. For most of the models, the skill for single-member (ensemble mean) hindcasts is less than the estimated predictability limit by about 5–10 days (15–25 days), implying that significantly more skillful MJO forecasts can be afforded through further improvements of dynamical models and ensemble prediction systems (EPS).

Corresponding author address: J. M. Neena, Jet Propulsion Laboratory, 4800 Oak Grove Drive, MS 233-300, Pasadena, CA 91109.
E-mail: neena.j.mani@jpl.nasa.gov

1. Introduction

In the tropics, between the weather and the seasonal time scales there is a dominant mode of intraseasonal variability known as the Madden–Julian oscillation (MJO; Madden and Julian 1971; Zhang 2005). It represents a primary source of predictability on the intraseasonal time scales and also modulates and influences different scales of atmospheric and oceanic variability over the tropics and extratropics (Maloney and Hartmann 2000a,b; Jones and Carvalho 2002; Zhang and Gottschalck 2002; and many others). Hence, the effective prediction of MJO can provide insight into the statistical evolution or even extend the predictive skill of a wide range of phenomena from synoptic scale to the climate scale. This understanding has given significant impetus to better simulate and forecast the MJO using both dynamical and statistical methods (Waliser 2011). Initial efforts toward MJO prediction using dynamical models were marginally successful, with prediction skill ranging from 7 to 10 days (e.g., Jones et al. 2000; Seo et al. 2005), much less than that of the statistical models, which exhibited up to 2 weeks of prediction skill (e.g., Lo and Hendon 2000; Wheeler and Weickmann 2001; Jiang et al. 2008). On the other hand, attempts toward estimating the predictability of the MJO indicated a limit around 4 weeks, albeit with the models that were only marginally successful at replicating the MJO (e.g., Waliser et al. 2003; Reichler and Roads 2005; Waliser 2006a). Recent predictability estimates by Pegion and Kirtman (2008a) indicate even longer predictability for the MJO in coupled simulations.

Past multimodel assessments of model performance for the MJO (e.g., Slingo et al. 1996; Lin et al. 2006; Kim et al. 2009; Zhang et al. 2013) have indicated that inadequacies in cumulus parameterization schemes (e.g., Maloney and Hartmann 2001; Liu et al. 2005; Vitart et al. 2007), coarse vertical resolution (Slingo et al. 1996; Inness et al. 2001), and lack of air–sea coupling (e.g., Hendon 2000; Fu et al. 2007; Woolnough et al. 2007) were some of the factors limiting the simulation of the MJO by GCMs. In addition to these factors, MJO prediction using numerical weather prediction models are further affected by the uncertainties in initial conditions arising from observational errors and errors in the assimilation systems (Agudelo et al. 2009; Fu et al. 2011). Through better model parameterizations, increased vertical resolution, improved assimilation methodology and observation availability, and in some cases the inclusion of ocean coupling (e.g., Fu et al. 2003; Fu and Wang 2004; Woolnough et al. 2007; Zheng et al. 2004; Pegion and Kirtman 2008b), commendable improvements have been made in the past decade in MJO simulation and prediction (Waliser 2011). Specifically, the

studies by Vitart and Molteni (2010), Rashid et al. (2011), Seo et al. (2009), and Kang and Kim (2010) have shown that skillful prediction of the boreal winter MJO can be made up to 2–3 weeks in advance.

The developments highlighted above call for a systematic evaluation of the present-day MJO dynamical prediction capabilities, particularly in light of continued and emerging interests in subseasonal prediction (e.g., Vitart et al. 2012; Brunet et al. 2010; Moncrieff et al. 2012) and gains made in model fidelity (Zhang et al. 2013; Zhang and Van den Dool 2012). While assessments of MJO forecast skill are often performed by different modeling centers, the forecast set ups, approaches for isolating MJO signals, and prediction skill metrics are often diverse which do not afford a comprehensive and uniform assessment. To address this need, the Asian Pacific Climate Center (APCC), the World Climate Research Programme (WCRP)–World Weather Research Programme (WWRP)/The Observing System Research and Predictability Experiment (THORPEX) Year of Tropical Convection (YOTC) Project and MJO Task Force, and the National Oceanic and Atmospheric Administration (NOAA) Climate Test Bed have developed and supported the Intraseasonal Variability Hindcast Experiment (ISVHE), which called for an extended-range, multimodel hindcast dataset specifically targeting at the ISV. The broad objectives of the ISVHE are to assess the forecast skill and predictability of the ISV including the MJO and related phenomena, in a multimodel framework, and to develop optimal strategies for multimodel ensemble (MME) prediction of the ISV. In a companion study, J.-Y. Lee et al. (2014, unpublished manuscript) provide an overview of the ISVHE and analyses the hindcast skill of the participating models. Specifically, they evaluate the prediction skill of the boreal winter MJO using the ISVHE multimodel hindcasts based on the real-time multivariate MJO (RMM) indices (Wheeler and Hendon 2004, hereafter WH04). The possibility of multimodel ensemble prediction for the MJO is also explored in that study, with the result that even simply constructed multimodel ensembles were found to yield a prediction skill out to 4 weeks.

In contrast to examinations of prediction skill, there are fewer attempts to characterize the predictability of the MJO, particularly using contemporary general circulation models (GCMs; Waliser 2011). One of the earlier attempts for estimating MJO predictability was made by Waliser et al. (2003) using "perfect model forecasts" with the National Aeronautics and Space Administration (NASA) Goddard Laboratory for Atmospheres (GLA) atmospheric GCM (AGCM). It was

demonstrated that, for 200-hPa velocity potential, the MJO predictability extended out to about 25–30 days and to about 10–15 days for precipitation. Later, Reichler and Roads (2005), using the National Centers for Environmental Prediction (NCEP) seasonal forecast model, estimated the MJO predictability in 200-hPa velocity potential field to be about 4 weeks when the model, initial, and boundary conditions were all perfect. However, these estimates were based on AGCMs with marginal ability to represent the MJO (Waliser 2006a). Also, in these studies, the predictability of MJO was analyzed in different dynamical fields (e.g., winds and precipitation), and, as in the case of prediction skill estimates, diverse approaches were often adopted for isolating the MJO signal. Later studies (e.g., Fu et al. 2007, 2008; Pegion and Kirtman 2008a) that investigated the role of air–sea coupling on MJO predictability, using different coupling configurations, revealed a longer MJO predictability in fully coupled atmosphere–ocean models. Based on an estimate of predictability involving ensemble means, using the NCEP Climate Forecast System (CFS; Saha et al. 2006), Pegion and Kirtman (2008a) showed that the predictability of MJO extends beyond 45 days. These predictability estimates based on individual GCMs were dependent on how well the MJO was captured by the models. The present-day dynamical models have shown marked improvement in the representation of the MJO, and hence it is worth an attempt to explore MJO predictability in present-day GCMs and across different GCMs.

In the present study, we explore and characterize the predictability of the boreal winter MJO based on the ISVHE coupled model hindcasts using a common methodology to quantify the gap between the present-day prediction skill and predictability of the MJO. The details of the ISVHE dataset and the methodology for isolating the MJO from model hindcasts and estimating its predictability are provided in sections 2 and 3. The predictability estimates from the eight models, including the dependence of predictability on the amplitude and phase of MJO at hindcast initiation, are presented in section 4a. Analysis of whether the primary and secondary MJO events (Matthews 2008; Straub 2013) have different predictability is also explored in this section. The MJO prediction skills of the different models are compared against the predictability estimates in section 4b. A brief analysis of the ability of the different ensemble prediction systems (EPS) to take into account the total uncertainties from initial conditions and internal dynamics, and their efficiency in improving the deterministic prediction skill is illustrated in section 4c. A summary and conclusions from the present study are provided in section 5.

2. Hindcast data

The ISVHE was launched in 2009 and is jointly supported by the APCC, NOAA, Climate Variability and Predictability (CLIVAR) Asian–Australian Monsoon Panel, YOTC and MJO Task Force, and the Scientific Steering Committee of Asian Monsoon Years (2007–12). The ISVHE was designed to examine tropical intraseasonal variability as a whole, including the boreal winter MJO and the boreal summer intraseasonal oscillation (ISO) (e.g., Waliser 2006b). It consists of two sets of experiments: 1) long "control" simulations (20 yr) to examine the participating models ability to represent the intrinsic ISV modes and 2) hindcasts of at least 45-day durations, initiated on the 10th day of every calendar month (such that a large number of independent MJO events are captured) and spanning about 20 yr. All the participating models have mostly adhered to the guidelines set down by the ISHVE in generating the hindcasts. However, there are some differences in the ensemble generation approaches followed by different modeling centers and in the number of ensembles. While some modeling centers used time-lagged initial conditions (Hoffman and Kalnay 1983) for ensemble generation, others adopted the singular vector (Buizza and Palmer 1995; Molteni et al. 1996) or bred vector (Toth and Kalnay 1993, 1997) approaches. In this study, we have analyzed the hindcasts for the winter season (November–March) from eight coupled models from six centers, which include two versions of the Australian Bureau of Meteorology coupled model (ABOM1 and ABOM2), two versions of the NCEP/Climate Prediction Center (CPC) coupled models (CFS1 and CFS2), the European Centre for Medium-Range Weather Forecasts (ECMWF) model, the Japan Meteorological Agency (JMA) coupled model (JMAC), the coupled model of Euro-Mediterranean Center on Climate Change (CMCC), and the Seoul National University (SNU) coupled model (SNUC). Table 1 gives the details of hindcast datasets from the eight models. Further details of the ISVHE and the participating models can be found in J.-Y. Lee et al. (2014, unpublished manuscript). Daily averaged outgoing longwave radiation (OLR) data from NOAA polar-orbiting series of satellites (Liebmann and Smith 1996) and wind fields from the NCEP–National Center for Atmospheric Research (NCAR) reanalysis dataset (Kalnay et al. 1996) represent the observed fields.

3. Methodology

To estimate predictability or prediction skill of the MJO, it is necessary to isolate the MJO signal. Earlier approaches for isolating the MJO in model hindcasts often involved applying bandpass filtering after appending

TABLE 1. Details of hindcast data from the eight models used in this study.

	Model(s)	Hindcast details	Ensemble size nk (ensemble generation method)
ABOM1 (Colman et al. 2005)	Predictive Ocean–Atmosphere Model for Australia (POAMA) 1.5 [Australian Community Ocean Model, version 2 (ACOM2), and Bureau of Meteorology Research Centre (BMRC) Atmospheric Model (BAM3)]	160-day hindcasts, 1980–2006: initialized 1st day of every month	10 (6-h lagged atmospheric initial conditions)
ABOM2 (Cottrill et al. 2013)	POAMA 2.4 (ACOM2 and BAM3)	100-day hindcasts, 1989–2009: initialized 1st and 11th day of every month	11 (perturbations using coupled bred vectors)
CMCC (Scoccimarro et al. 2011)	ECHAM5 and Océan Parallélisé 8.2 (OPA8.2)	59-day hindcasts, 1989–2007: initialized 1st, 11th and 21st day of every month	5 (1-day lagged initial conditions)
ECMWF (Alves et al. 2004; Vialard et al. 2005)	Integrated Forecast System (IFS) and Hamburg Ocean Primitive Equation Model (HOPE)	56-day hindcasts, 1989–2008: initialized 1st day of every month	5 (different oceanic initial conditions)
JMAC (JMA 2007; Ishikawa et al. 2005)	JMA coupled GCM (CGCM)	61-day hindcasts, 1989–2008: initialized every 15th day	5 (perturbations using singular vectors)
CFS1 (Saha et al. 2006)	NCEP/CPC CFS, version 1 [Global Forecast System (GFS) and Modular Ocean Model version 3 (MOM3)]	70-day hindcasts, 1981–2008: initialized 2nd, 12th, and 22nd day of every month	5 (1-day lagged initial conditions)
CFS2 (Saha et al. 2014)	NCEP/CPC CFS, version 2 (GFS and MOM3)	44-day hindcasts, 1999–2010: Initialized 1st, 11th, and 21st day of every month	4 (6-h lagged initial conditions)
SNUC (Kug et al. 2008)	SNU coupled model (SNU AGCM and MOM3)	45-day hindcasts, 1990–2008: Initialized 1st, 11th, and 21st day of every month	4 (6-h lagged initial conditions)

observed data or model control simulation data before the start of the model hindcasts (e.g., Jones et al. 2000). After the introduction of the RMM indices by WH04, which are based on an empirical orthogonal function (EOF) analysis of the combined fields of equatorially averaged 850- and 200-hPa zonal wind (U850 and U200), and NOAA OLR, isolation of the MJO mode became possible without relying on time filtering. Recently, different variations of the WH04 method were used in MJO prediction studies (Vitart et al. 2007; Lin et al. 2008; Seo et al. 2009). While some studies defined the RMM indices based on the observed MJO modes, others defined the indices based on the intrinsic MJO modes derived from model control runs. Since the intrinsic MJO-like variability differs greatly in the ISVHE participating models, the second approach would not suit our objective of evaluating the MJO predictability using a common metric. Hence, we use the observed MJO mode following WH04 to isolate the MJO signals in the model hindcasts (Gottschalck et al. 2010; Sperber and Waliser 2008).

Starting from the daily hindcast fields of OLR, U850, and U200 of any model, the corresponding model hindcast climatologies are removed to obtain the bias corrected anomaly fields. Following the WH04 methodology, the interannual variability is further removed by subtracting the previous 120-day mean (computed by appending the corresponding observed anomaly fields before the hindcast anomaly fields) from each day's anomaly fields (Gottschalck et al. 2010). We have verified that removing or retaining the interannual variability in the anomalies does not qualitatively affect the predictability estimates made in the study. The OLR, U850, U200 anomalous fields are then latitudinally averaged between 15°S and 15°N and normalized by their respective zonal average values of temporal standard deviations (again obtained from the observed fields). Then the combined fields are projected on to the WH04 combined EOF modes to obtain the MJO principal component time series, RMM1 and RMM2, which represent the MJO signal in the model hindcast. The observed RMM1 and RMM2 values are computed in a similar way using observed fields of OLR, U850, and U200. Both the observed and hindcast RMM indices are further normalized by the standard deviation of the observed RMM indices.

Two approaches are adopted for measuring the predictability of MJO in the hindcasts. Both estimates of predictability are based on the perfect model assumption.

By perfect model forecasts or "identical twin forecasts," we mean the forecasts made using the same model from a control initial condition and a "perturbed" initial condition (obtained by perturbing the control initial condition) (e.g., Lorenz 1982). In the first method, which we call the single-member estimate, the RMM1 and RMM2 values from any given hindcast ensemble member are considered as the control MJO forecast and those from every other ensemble member are considered as perturbed MJO forecasts. The divergence of these MJO trajectories is calculated as a function of forecast lead. The error is defined as the difference in forecast RMM1 and RMM2 between the hindcast deemed control and each other ensemble member, as a function of lead time. The error estimate formulation includes the contributions from both RMM1 errors as well as the RMM2 errors [see Eq. (1)] and is similar to the bivariate MJO metric for prediction skill estimation employed by Lin et al. (2008). Predictability is defined as the lead time at which the difference or error from the perfect model hindcasts becomes as large as the average MJO amplitude in the hindcasts. This method is similar to the methodology used in earlier studies (e.g., Waliser et al. 2003; Liess et al. 2005; Fu et al. 2007, 2008; Pegion and Kirtman 2008a), except we use the RMMs of the hindcast in place of the time filtering of specific fields adopted in that study.

Consider a model that produces J day-long ensemble hindcasts (ensemble size nk) for N different initial conditions spanning the November–March period of nyr years. For a particular initial condition i at lead time j, the error (the difference in RMM values for any two ensemble member hindcasts k_1 and k_2) is defined as

$$E_{ij}^2 = (RMM1_{ij}^{k_1} - RMM1_{ij}^{k_2})^2 \\ + (RMM2_{ij}^{k_1} - RMM2_{ij}^{k_2})^2. \quad (1)$$

Here k_1 represents the control and k_2 represents the perturbed forecast. The signal is computed from all the control forecasts (k_1) and defined as the average MJO variance in a 51-day sliding window, as a function of lead time. The observed RMM values prior to hindcast initiation day were also used in the sliding window computation of MJO variance. A 51-day window was chosen to cover a full MJO cycle; however, there is not much sensitivity of the signal estimate on the window size. The signal corresponding to a particular initial condition i at lead time j is computed by setting $L = 25$ in Eq. (2),

$$S_{ijk_1}^2 = \frac{1}{2L+1} \sum_{t=-L}^{L} (RMM1_{ij+t}^{k_1})^2 + (RMM2_{ij+t}^{k_1})^2. \quad (2)$$

The mean-square error for each lead day j is computed over a total $N \times m_1$ cases [m_1 control–perturbed (k_1–k_2) pairs for a given initial condition, over N different initial conditions]. For the single-member predictability estimate m_1 takes the value of nk − 1 factorial when all the ensemble members are initialized the same day, while it counts only those ensemble pairs initialized within a maximum separation of 1 day when the ensemble members are initialized from time-lagged initial conditions,

$$\langle E_j^2 \rangle = \frac{1}{N \times m_1} \sum_{i=1}^{N} \sum_{m_1 \text{ perfect model pairs}} E_{ij}^2, \quad (3)$$

and the mean signal for each lead day j is computed over a total $N \times$ nk cases,

$$\langle S_j^2 \rangle = \frac{1}{N \times \text{nk}} \sum_{i=1}^{N} \sum_{k_1=1}^{\text{nk}} S_{ijk_1}^2. \quad (4)$$

The single-member estimate of predictability is defined as the lead time at which the mean-square error becomes as large as the mean signal: in other words, the time lead at which small errors in initial conditions would become as large as the modeled standard deviation of the MJO.

While this method estimates the predictability from the individual hindcasts, we also attempt to estimate the predictability of ensemble-mean hindcasts using a slight alteration. Pegion and Kirtman (2008a) have shown that the predictability of MJO associated with ensemble means is longer than the predictability associated with individual ensemble members. In the second method, which we call the ensemble estimate, in the place of measuring the error growth between two ensemble member forecasts, the error growth is estimated for a single ensemble member (control) and the ensemble mean over all the other ensemble members (perturbed). In Eq. (2), the superscript k_2 would represent the RMM1 and RMM2 values averaged over all the ensemble members other than k_1. In computing the mean-square error, m_1 takes the value of ensemble size nk. The signal estimate is same as that for the first method. To be consistent with the predictability estimation, the average MJO hindcast skill is also measured in a similar way as the predictability estimate, substituting the observed RMM values in place of k_2 in Eq. (1). Signal is computed from the observed RMMs using Eq. (2). Ensemble-mean hindcast skill is computed in a similar way using only the ensemble-mean hindcast (averaged over all ensemble members). The overall approach described above is driven by this study's primary objective of estimating the predictability of the MJO, with a secondary objective of
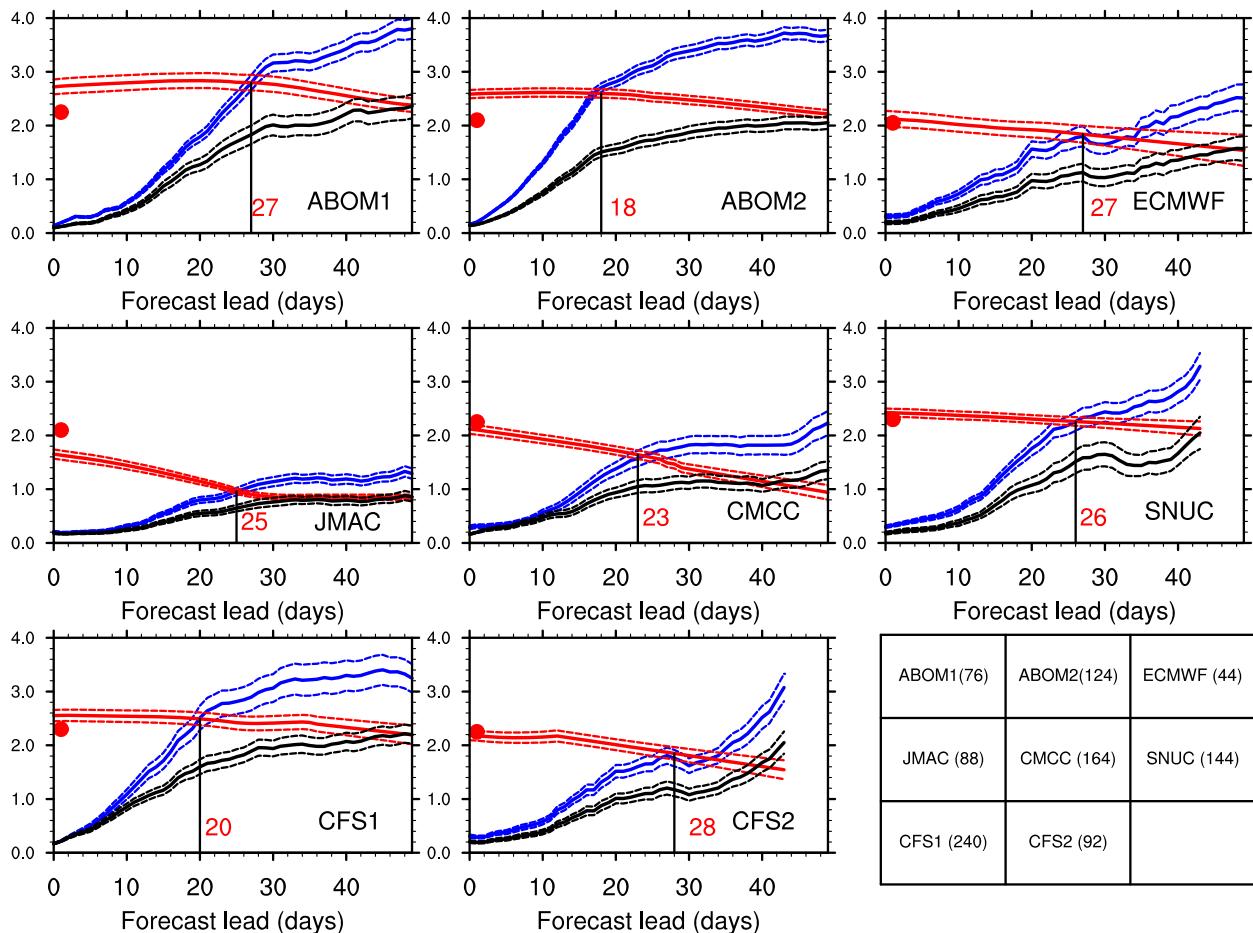
FIG. 1. Average error and signal estimates for the eight models for strong MJO initial conditions. Saturation of the blue solid error growth curve (single-member estimate) with respect the signal (red solid) marks the MJO predictability for individual forecasts (denoted by the black vertical line along with the corresponding number of forecast lead day in red in each panel) and saturation of the black solid error growth curve (ensemble-mean estimate) with respect the signal (red solid) marks the MJO potential predictability for ensemble-mean forecasts. Also shown as dashed lines are the 95% confidence estimates of error and signal. The solid red circle in each panel represents the signal estimates based on observations. The table at the bottom-right gives the number of cases (N), corresponding to strong MJO events at the time of initiation, used in the predictability estimates for each model.

comparing the predictability estimate from each model with its corresponding prediction skill but using a common framework for the comparison.

4. Results and discussion

a. MJO predictability estimates

The predictability of the MJO was examined for the eight models using the two approaches described above. In Fig. 1, the average error (blue: single member method; black: ensemble method) and average signal estimates (red) are shown as a function of lead time for all the hindcasts initiated from "strong" MJO events. This means that in computing the average error and average signal for any given model, hindcasts were only

included if the observed MJO amplitude, defined as $(RMM1^2 + RMM2^2)^{1/2}$, was greater than 1.0 on day 0 of the hindcast. Also, to ensure that the predictability estimates are not influenced by a bias in relative number of cases in each MJO phase, an equal number of hindcasts n were included in the predictability estimation for each pair of MJO phases (phases 8 and 1, 2 and 3, 4 and 5, and 6 and 7). Here, n was determined from the minimum of the number of hindcasts occurring in the four groups. The table in the bottom right corner of Fig. 1 gives the total number of cases [N in Eqs. (3) and (4)] used in predictability estimation, where $N = 4n$. To give an idea of how well the MJO signal in the model hindcasts compares with the observed, the day-0 value of the average signal computed from observed RMMs is indicated by a solid red circle in each panel of Fig. 1. Based
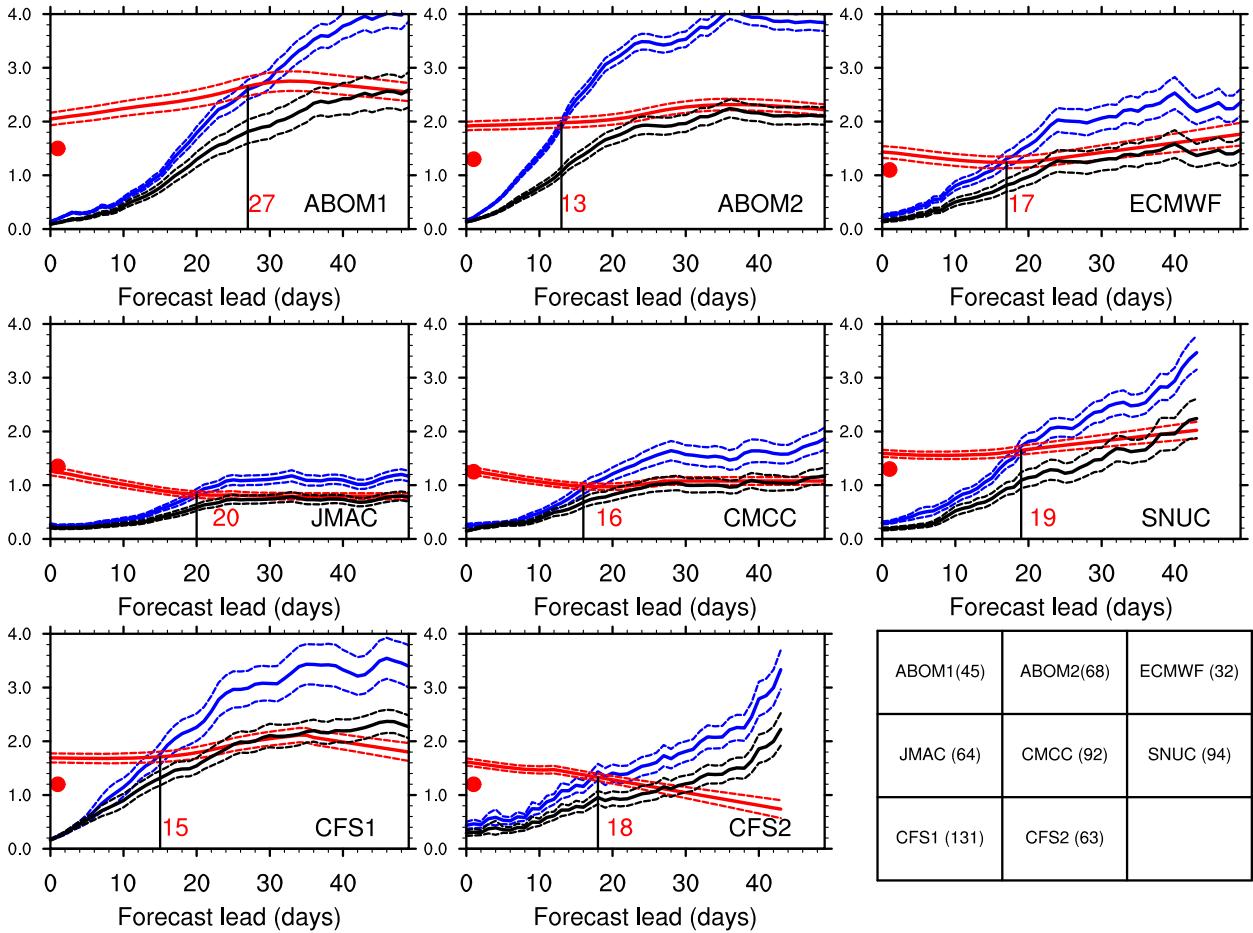
FIG. 2. As in Fig. 1, but for model hindcasts from weak MJO initial conditions.

on Fig. 1, the single-member estimate of MJO predictability is obtained from the lead time at which the (blue) error curve becomes as large as the (red) signal; similarly, the ensemble estimate of MJO predictability is obtained as when the (black) ensemble error curve becomes as large as the (red) signal. In six of the eight models (except ABOM2 and CFS1), for both the single-member and ensemble estimates, exponential error growth is evident with a slower error growth phase for the first few days of hindcast followed by a phase of faster error growth. The single-member predictability estimates of these six models exhibits a range of 24–30 days. In the other two models, ABOM2 and CFS1, the error growth curve has a more linear character, with abrupt error growth starting from day 1. The resulting estimate of single-member predictability from these two models is slightly lower, around 20 days. The differences in the error growth among different models with very similar values of initial error indicate that the error growth on the intraseasonal time scale is not dependent on the initial conditions alone but also could be governed

by the modeled processes themselves. In all the models, the predictability estimate for the ensemble mean is much higher than the estimate using single members. The ensemble estimate of predictability is more than 45 days for ABOM1, ABOM2, and ECMWF and around 35–45 days for all other models.

Figure 2 illustrates the same information as Fig. 1 but for cases of weak MJO events: namely, based on all cases when the MJO amplitude is less than 1.0 on day 0 of the hindcast. Again, the table in the bottom right corner of Fig. 2 gives the total number of cases [N in Eqs. (3) and (4)] associated with weak MJO initial conditions. It is seen that both the single-member and ensemble estimates of predictability are shorter than their respective counterparts for strong MJO cases, as shown in Fig. 1. The single-member predictability estimates are on the average lower by around 5–10 days for weak MJO events in all models except ABOM1, while for weak MJO cases the average ensemble estimate of predictability is around 20–30 days. The dependence of estimated predictability on MJO amplitude was also noted by Waliser et al. (2003).
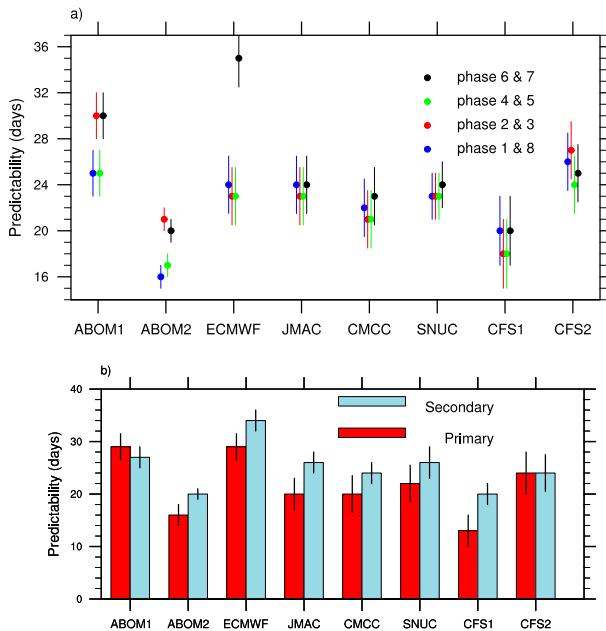
FIG. 3. MJO predictability (days) estimates for the eight models for (a) hindcasts initiated from different MJO phases and (b) primary and secondary MJO events. The error bars represent the 95% confidence interval for the predictability estimates.

Although the MJO is observed as a globally propagating signal in circulation, the zonal asymmetries in the surface boundary conditions, interactions, and character of convective signature (e.g., Hendon and Salby 1994) suggest the possibility that the MJO predictability may depend on its phase. Lin et al. (2008) demonstrated such a dependence on the phase of the MJO at initiation in their estimates of prediction skill. They showed that forecasts initialized with active convection over tropical Africa and the Indian Ocean sectors (phases 1–3) have higher skill than those initialized from other phases. Such an initial-phase dependence, however, was not clear in a similar study by Rashid et al. (2011). Hence, the dependence of MJO predictability on the location of MJO convection (identified from the eight RMM phases) at day 0 of hindcast is further examined using the single-member estimate method (Fig. 3a). While no significant dependence of predictability on initial MJO phase is found in most of the models examined here, the ABOM1, ABOM2, and ECMWF models exhibit some sensitivity of predictability on the initial MJO phase (Fig. 3a). For ABOM1 and ABOM2, the predictability is found to be slightly higher when initialized from MJO phases 2, 3, 6, and 7 as compared to those from phases 1, 8, 4, and 5. The difference in predictability between these two groups is significant at the 95% confidence level based on a Student's t test. For the ECMWF model,

hindcasts initialized from MJO phase 6 or 7 tend to have significantly higher predictability than the rest (95% confidence). The higher predictability for hindcasts initialized from MJO phases 2, 3, 6, and 7 may be related to the stronger MJO amplitude over the Indian Ocean and western Pacific. Another aspect of interest is that most models exhibit predictability beyond 20 days for hindcasts initiated from phases 2 and 3: that is, hindcasts involving convection in the Indian Ocean at lead 0 days and propagation into the western Pacific over the subsequent 2–4 weeks. Both the simulation and forecasting of MJO convection propagation across the Maritime Continent have been found to be a hurdle for the present-day GCMs (Inness et al. 2003; Inness and Slingo 2006; Vintzileos and Pan 2007) and it has been contemplated whether this difficulty arises from common modeling deficiencies or whether an actual "Maritime Continent prediction barrier" exists. The fact that in all the models the predictability associated with hindcasts initiated from phases 2 and 3 is as good as or even higher than the predictability associated with other MJO phases implies that the Maritime Continent prediction barrier might not be an actual predictability limitation. An examination of the differences in MJO predictability for different target MJO phases would shed more light on this problem. However, it would require a more extensive hindcast experiment setup, ideally with extended hindcasts initiated from each calendar day.

Next we examine whether the MJO predictability estimates obtained from Fig. 1 is affected by the nature of the MJO events represented in the hindcast initial conditions. By "nature," we mean whether the MJO event is part of a preceding MJO cycle (secondary events) or it marks the initiation of a new MJO cycle unrelated to any previous event (primary events). There have been very few attempts to objectively identify primary and secondary MJO events from observations (e.g., Matthews 2008; Straub 2013). Of these, Straub (2013) classified the observed MJO for the 1979–2012 period into primary, intensification, and secondary events based on the RMM indices. Since we have used the RMM indices for the predictability estimates in this study, we adopt the Straub (2013) classification to compare the predictability of primary and secondary MJO events in the ISVHE hindcasts. According to Straub (2013), a primary MJO event is defined as when the RMM amplitude becomes greater than 1.0 and remains so through four subsequent RMM phases, after being preceded by a period of <1.0 amplitude for at least 7 days without any counterclockwise motion of the RMM indices inside the unit circle. The final criterion ensures that there were absolutely no MJO precursor signals for a primary event. A secondary MJO event is

identified as when the RMM index enters a particular phase with amplitude greater than 1.0 after having propagated through at least two prior phases with amplitude greater than 1.0 and subsequently propagates through two successive phases with the greater than 1.0 amplitude. The number of primary initiation dates identified from observations was very few, as compared to the secondary and intensification cases. To have a better sample size for our estimates we have redefined the primary events by relaxing the final criteria used in Straub (2013). When estimating the predictability associated with primary and secondary MJO events based on each model, the error and signal were calculated by including only those hindcasts whose day 0 falls within the ±5-day interval of the primary and secondary initiation dates identified from observations. The ABOM2, ECMWF, JMAC, and CFS1 models display a higher predictability for secondary MJO events as compared to primary events (Fig. 3b). The differences in predictability for primary and secondary MJO events in these models were found to be significant at 95% confidence level using a Student's *t* test. The other four models do not show a significant difference in predictability for primary and secondary MJO events.

b. Prediction skill versus predictability

The MJO prediction skill of a given model is a measure of how well the model is able to mimic the observed MJO evolution and is limited by both the deficiencies in model formulation as well as the errors in prescribing the initial conditions. If we discard the errors resulting from model deficiencies (and thus have a perfect model), the maximum attainable prediction skill, now only sensitive to the errors in initial conditions, defines MJO predictability, which was addressed above. For each model, the MJO predictability estimates (from Fig. 1) are contrasted against their respective MJO prediction skill estimates (single member and ensemble mean) in Fig. 4. To readily compare our predictability and prediction skill estimates, the methodology is identical: except in the predictability case the control is a given ensemble member while in the prediction skill case the control is the observation. Please refer to sections 2 and 3 for details of prediction skill estimation. The ensemble-mean prediction skill (hatched bars) is higher than the average single-member prediction skill (black bars) in all models. This may be because ensemble averaging helps to remove some of the errors attributable to atmospheric instabilities that dominate the single-member (i.e., deterministic) forecasts. However, the extent to which the effects of initial uncertainties are reduced depends on the fidelity of the EPS. A ±5-day range for the
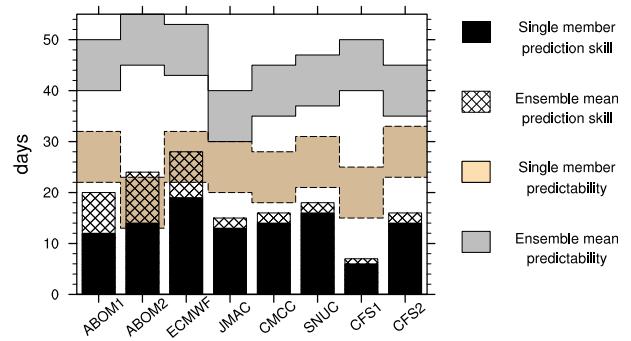

FIG. 4. The single-member prediction skill (black bar) and ensemble-mean prediction skill (hatched bar) estimates (days) for MJO for the eight models are shown along with their respective single-member (tan shaded area) and ensemble-mean (gray shaded area) estimates of MJO predictability (±5-day range).

single-member (ensemble) estimate of predictability is shown as the tan (gray) shaded area in Fig. 4.

Of the eight models, the ECMWF model shows the highest single-member prediction skill for MJO with useful skill up to 20 days and the CFS1 model has the least skill of about 6 days. All the other models exhibit skill ranging from 12 to 16 days. The upper limit of single-member predictability of MJO in most of the models falls in between 20 and 30 days. The predictability of MJO for ABOM2 and CFS1 has a lower range around 15–25 days. The ensemble-mean prediction skill is again highest for ECMWF (28 days) and ABOM2 (24 days) and is in the 15–20-day range for most of the other models. While the ensemble estimate of predictability is around 35–45 days in most models, ECMWF and ABOM2 exhibit slightly higher estimates of more than 45 days. The lowest range for ensemble estimate of predictability is observed in JMAC, around 30–40 days. These results are encouraging since it indicates that most of the present-day dynamic models have the scope for improving their MJO prediction skills by up to 2 weeks before reaching the upper limit of predictability. The large gap separating the single-member and ensemble estimates of predictability implies that effective strategies for ensemble prediction would play a major role in the improvement of MJO forecasts.

c. Spread–RMSE relation in different EPS

While the skill of the ensemble-mean forecast over the single-member skill would give a measure of the skill of the EPS, it is equally important to measure the uncertainty information contained in the ensemble member forecasts. Different approaches and metrics are used for evaluating the uncertainty information contained in ensemble forecasts [for a review, see Candille and Talagrand (2005)]. Evaluating the statistical consistency of the ensemble is one of the simpler approaches (Murphy
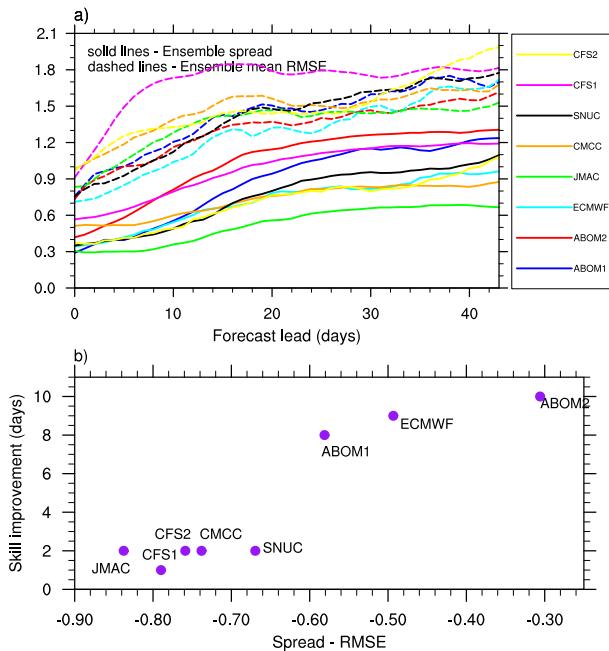
FIG. 5. (a) Bivariate measure of ensemble spread (solid lines) and ensemble-mean RMSE (dashed lines) for the MJO in the different EPSs. (b) The 25-day forecast lead average of the spread minus RMSE values [set of solid and dashed curves in (a)] for each model, plotted against the corresponding values of skill improvement (day) in ensemble means over single-member forecasts (width of hatched area in Fig. 4).

1973). In a statistically consistent ensemble, the root-mean-square error (RMSE) of the ensemble mean (computed over a sufficiently large sample) will be equal to the ensemble standard deviation (ensemble spread) (Whitaker and Loughe 1998) at all forecast leads. The relationship between the ensemble spread and the ensemble-mean RMSE for the MJO is explored in the eight models. Both estimates were made following the form suited for finite size ensembles as defined by Leutbecher and Palmer (2008).

For each hindcast initial condition and each forecast lead day, a bivariate measure of the ensemble spread for MJO is defined as the combined standard deviations of the RMM1 and RMM2 values in the ensemble member hindcasts about their respective ensemble-mean values, and the average is computed over all winter initial conditions (similar to the error and signal estimation). The bivariate measure of the ensemble-mean RMSE for MJO is estimated by computing the root-mean-square difference between the observed and forecasted RMM values in ensemble-mean hindcasts (following Lin et al. 2008). Figure 5a shows the ensemble spread (solid lines) and ensemble-mean RMSE (dotted lines) estimates as a function of hindcast lead for the eight EPSs. The spread is lower than the RMSE in all models, indicating

that all the EPSs are underdispersive for the MJO. An underdispersive ensemble is one that does not account for all sources of error from internal dynamics (Buizza et al. 1999). The level of dispersion in the different EPS can be measured from the closeness of the spread (solid curves) and RMSE (dashed curves) values. From Fig. 5a, it can be seen that these two curves are closest to each other for ABOM2. For better comprehension of the level of dispersion in the eight EPSs in Fig. 5a, the average difference between the spread and RMSE (from Fig. 5a) for the first 25 days of hindcast is plotted against the skill of the EPS in Fig. 5b. The skill of the EPS is defined as the improvement of ensemble-mean prediction skill over single-member prediction skill (hatched area in Fig. 4). A smaller negative value on the x axis of Fig. 5b reflects a better dispersed EPS for the MJO. By this measure, ABOM2, ECMWF, and ABOM1 exhibit relatively better dispersed EPSs and are associated with higher ensemble-mean skill. In a recent study, Hudson et al. (2013) have shown how the coupled bred vector ensemble generation approach in ABOM2 produces better dispersed ensembles as compared to ABOM1. They also argue that lagged atmospheric initial conditions as in ABOM1 can often lead to underdispersion of ensembles. While this difference in level of dispersion between ABOM1 and ABOM2 holds well in our analysis, much higher levels of underdispersion are observed in the other models that have used widely different approaches for ensemble generation. However, we would refrain from making any further comparisons or conclusions at this stage.

5. Summary and conclusions

The predictability of boreal winter MJO (November–March) is investigated by analyzing hindcasts from eight GCMs participating in the ISVHE initiative. The MJO in the hindcasts were extracted by projecting the hindcast OLR and 850- and 200-hPa wind fields on to the observed WH04 combined EOFs. MJO predictability was assessed based on these RMM values. For a given model, the ensemble hindcasts are considered as a pool of "control" and "perturbed" hindcasts. Measuring the divergence of MJO in a pair of ensemble member hindcasts is considered equivalent to measuring the divergence of MJO in a perfect model setup. The signal to noise ratio method for predictability estimation used by previous studies like Waliser et al. (2003), Liess et al. (2005), and Fu et al. (2007, 2008) is adopted in this study. Two approaches are used to estimate the MJO predictability: that is, the single-member estimate and the ensemble estimate. Single-member predictability was derived from the divergence of ensemble member hindcast

pairs: one of which is treated as the control and the other is treated as the perturbed. When assessing ensemble predictability, the divergence of an ensemble member hindcast is measured with respect to the ensemble-mean hindcast of all other ensemble members. On an average, a 20–30-day MJO single-member predictability is exhibited in the collection of the eight ISVHE models and the ensemble estimate of MJO predictability is often between 35 and 45 days (Fig. 4). The dependence of the predictability estimates on the MJO amplitude and phase during hindcast initiation shows a lower predictability (often by 5–10 days) for hindcasts initiated from weak MJO conditions (Fig. 2), as compared to those initiated from strong MJO conditions (Fig. 1). A systematic phase dependency was not observed in all models. The ABOM1, ABOM2, and ECMWF models exhibited some phase dependence with slightly higher predictability for hindcasts initiated from MJO phases 2, 3, 6, or 7 (Fig. 3a). It was also noted that in most models the predictability associated with hindcasts initiated from phases 2 and 3 was equal to or even higher that the predictability associated with the other MJO phases, giving a range of around 20 days. This implies that the so-called Maritime Continent prediction barrier may not be an intrinsic predictability limitation. The predictability of primary and secondary MJO events was also examined based on the classification by Straub (2013). Four of the eight models showed a higher predictability for secondary MJO events as compared to primary events (Fig. 3b). Comparison of the predictability estimates with the prediction skill of the models reveals that, for all models, the present-day single-member prediction skills can be further improved by at least 1 week before achieving the single-member predictability limit. The relation between ensemble spread and ensemble-mean RMSE for the MJO was also analyzed in the eight EPSs. While all the EPSs were found to be underdispersed for the MJO, the EPSs of the ABOM2, ECMWF, and ABOM1 models were found to be the ones relatively better dispersed for the MJO, and this is also reflected in the better MJO prediction skill for these models. The results indicate that, in addition to the efforts toward model and initial condition improvements, dedicated efforts should also be directed toward developing better ensemble prediction strategies. The notable differences in MJO prediction skill brought out by tailored ensemble prediction approaches for the MJO (e.g., Ham et al. 2012; Chikamoto et al. 2007) point to the open areas of research for further extending the MJO prediction capabilities using dynamical models.

REFERENCES

Agudelo, P. A., C. D. Hoyos, P. J. Webster, and J. A. Curry, 2009: Application of a serial extended forecast experiment using the ECMWF model to interpret the predictive skill of tropical intraseasonal variability. *Climate Dyn.,* **32,** 855–872, doi:10.1007/s00382-008-0447-x.

Alves, O., M. Balmaseda, D. Anderson, and T. Stockdale, 2004: Sensitivity of dynamical seasonal forecasts to ocean initial conditions. *Quart. J. Roy. Meteor. Soc.,* **130,** 647–668, doi:10.1256/qj.03.25.

Brunet, G., and Coauthors, 2010: Collaboration of the weather and climate communities to advance subseasonal to seasonal prediction. *Bull. Amer. Meteor. Soc.,* **91,** 1397–1406, doi:10.1175/2010BAMS3013.1.

Buizza, R., and T. N. Palmer, 1995: The singular-vector structure of the atmospheric global circulation. *J. Atmos. Sci.,* **52,** 1434–1456, doi:10.1175/1520-0469(1995)052<1434:TSVSOT>2.0.CO;2.

——, M. Miller, and T. N. Palmer, 1999: Stochastic representation of model uncertainties in the ECMWF ensemble prediction system. *Quart. J. Roy. Meteor. Soc.,* **125,** 2887–2908, doi:10.1002/qj.49712556006.

Candille, G., and O. Talagrand, 2005: Evaluation of probabilistic prediction systems for a scalar variable. *Quart. J. Roy. Meteor. Soc.,* **131,** 2131–2150, doi:10.1256/qj.04.71.

Chikamoto, Y., H. Mukougawa, T. Kubota, H. Sato, A. Ito, and S. Maeda, 2007: Evidence of growing bred vector associated with the tropical intraseasonal oscillation. *Geophys. Res. Lett.,* **34,** L04806, doi:10.1029/2006GL028450.

Colman, R., and Coauthors, 2005: BMRC Atmospheric Model (BAM) version 3.0: Comparison with mean climatology. BMRC Research Rep. 108, 23 pp.

Cottrill, A., and Coauthors, 2013: Seasonal forecasting in the Pacific using the coupled model POAMA-2. *Wea. Forecasting,* **28,** 668–680, doi:10.1175/WAF-D-12-00072.1.

Fu, X., and B. Wang, 2004: Differences of boreal summer intraseasonal oscillations simulated in an atmosphere–ocean coupled model and an atmosphere-only model. *J. Climate,* **17,** 1263–1271, doi:10.1175/1520-0442(2004)017<1263:DOBSIO>2.0.CO;2.

——, ——, T. Li, and J. McCreary, 2003: Coupling between northward-propagating, intraseasonal oscillations and sea surface temperature in the Indian Ocean. *J. Atmos. Sci.,* **60,** 1733–1753, doi:10.1175/1520-0469(2003)060<1733:CBNIOA>2.0.CO;2.

——, ——, D. E. Waliser, and L. Tao, 2007: Impact of atmosphere–ocean coupling on the predictability of monsoon intraseasonal oscillations. *J. Atmos. Sci.,* **64,** 157–174, doi:10.1175/JAS3830.1.

——, B. Yang, Q. Bao, and B. Wang, 2008: Sea surface temperature feedback extends the predictability of tropical intraseasonal oscillation. *Mon. Wea. Rev.,* **136,** 577–597, doi:10.1175/2007MWR2172.1.

——, B. Wang, J.-Y. Lee, W. Wang, and L. Gao, 2011: Sensitivity of dynamical intraseasonal prediction skills to different initial conditions. *Mon. Wea. Rev.,* **139,** 2572–2592, doi:10.1175/2011MWR3584.1.

Gottschalck, J., and Coauthors, 2010: A framework for assessing operational Madden–Julian oscillation forecasts: A CLIVAR MJO Working Group project. *Bull. Amer. Meteor. Soc.,* **91,** 1247–1258, doi:10.1175/2010BAMS2816.1.

Ham, Y.-G., S. Schubert, and Y. Chang, 2012: Optimal initial perturbations for ensemble prediction of the Madden–Julian oscillation during boreal winter. *J. Climate,* **25,** 4932–4945, doi:10.1175/JCLI-D-11-00344.1.

Hendon, H. H., 2000: Impact of air–sea coupling on the MJO in a GCM. *J. Atmos. Sci.,* **57,** 3939–3952, doi:10.1175/1520-0469(2001)058<3939:IOASCO>2.0.CO;2.

——, and M. L. Salby, 1994: The life cycle of the Madden–Julian oscillation. *J. Atmos. Sci.,* **51,** 2225–2237, doi:10.1175/1520-0469(1994)051<2225:TLCOTM>2.0.CO;2.

Hoffman, R. N., and E. Kalnay, 1983: Lagged average forecasting, an alternative to Monte Carlo forecasting. *Tellus,* **35A,** 100–118, doi:10.1111/j.1600-0870.1983.tb00189.x.

Hudson, D., A. G. Marshall, Y. Yin, O. Alves, and H. H. Hendon, 2013: Improving intraseasonal prediction with a new ensemble generation strategy. *Mon. Wea. Rev.,* **141,** 4429–4449, doi:10.1175/MWR-D-13-00059.1.

Inness, P. M., and J. M. Slingo, 2006: The interaction of the Madden–Julian oscillation with the maritime continent in a GCM. *Quart. J. Roy. Meteor. Soc.,* **132,** 1645–1667, doi:10.1256/qj.05.102.

——, ——, S. J. Woolnough, R. B. Neale, and V. D. Pope, 2001: Organization of tropical convection in a GCM with varying vertical resolution: Implication for the simulation of the Madden-Julian oscillation. *Climate Dyn.,* **17,** 777–793, doi:10.1007/s003820000148.

——, ——, E. Guilyardi, and J. Cole, 2003: Simulation of the Madden–Julian oscillation in a coupled general circulation model. Part I: Comparisons with observations and an atmosphere-only GCM. *J. Climate,* **16,** 345–364, doi:10.1175/1520-0442(2003)016<0345:SOTMJO>2.0.CO;2.

Ishikawa, I., H. Tsujino, M. Hirabara, H. Nakano, T. Yasuda, and H. Ishizaki, 2005: Meteorological Research Institute Community Ocean Model (MRI.COM) manual (in Japanese). Meteorological Research Institute Tech Rep. 47, 189 pp.

Japan Meteorological Agency, 2007: Outline of operational numerical weather prediction at the Japan Meteorological Agency. WMO Numerical Weather Prediction Progress Rep. Appendix, 199 pp.

Jiang, X., D. E. Waliser, M. C. Wheeler, C. Jones, M. I. Lee, and S. D. Schubert, 2008: Assessing the skill of an all-season statistical forecast model for the Madden–Julian oscillation. *Mon. Wea. Rev.,* **136,** 1940–1956, doi:10.1175/2007MWR2305.1.

Jones, C., and L. M. V. Carvalho, 2002: Active and break phases in the South American monsoon system. *J. Climate,* **15,** 905–914, doi:10.1175/1520-0442(2002)015<0905:AABPIT>2.0.CO;2.

——, D. E. Waliser, J.-K. E. Schemm, and W. K. M. Lau, 2000: Prediction skill of the Madden and Julian oscillation in dynamical extended range forecasts. *Climate Dyn.,* **16,** 273–289, doi:10.1007/s003820050327.

Kalnay, E., and Coauthors, 1996: The NCEP/NCAR 40-Year Reanalysis Project. *Bull. Amer. Meteor. Soc.,* **77,** 437–471, doi:10.1175/1520-0477(1996)077<0437:TNYRP>2.0.CO;2.

Kang, I.-S., and H.-M. Kim, 2010: Assessment of MJO predictability for boreal winter with various statistical and dynamical models. *J. Climate,* **23,** 2368–2378, doi:10.1175/2010JCLI3288.1.

Kim, D., and Coauthors, 2009: Application of MJO simulation diagnostics to climate models. *J. Climate,* **22,** 6413–6436, doi:10.1175/2009JCLI3063.1.

Kug, J.-S., I.-S. Kang, and D.-H. Choi, 2008: Seasonal climate predictability with tier-one and tier-two prediction systems. *Climate Dyn.,* **31,** 403–416, doi:10.1007/s00382-007-0264-7.

Leutbecher, M., and T. N. Palmer, 2008: Ensemble forecasting. *J. Comput. Phys.,* **227,** 3515–3539, doi:10.1016/j.jcp.2007.02.014.

Liebmann, B., and C. A. Smith, 1996: Description of a complete (interpolated) outgoing longwave radiation dataset. *Bull. Amer. Meteor. Soc.,* **77,** 1275–1277.

Liess, S., D. E. Waliser, and S. Schubert, 2005: Predictability studies of the intraseasonal oscillation with the ECHAM5 GCM. *J. Atmos. Sci.,* **62,** 3320–3336, doi:10.1175/JAS3542.1.

Lin, H., G. Brunet, and J. Derome, 2008: Forecast skill of the Madden–Julian oscillation in two Canadian atmospheric models. *Mon. Wea. Rev.,* **136,** 4130–4149, doi:10.1175/2008MWR2459.1.

Lin, J.-L., and Coauthors, 2006: Tropical intraseasonal variability in 14 IPCC AR4 climate models. Part I: Convective signals. *J. Climate,* **19,** 2665–2690, doi:10.1175/JCLI3735.1.

Liu, P., B. Wang, K. R. Sperber, T. Li, and G. A. Meehl, 2005: MJO in the NCAR CAM2 with the Tiedtke convective scheme. *J. Climate,* **18,** 3007–3020, doi:10.1175/JCLI3458.1.

Lo, F., and H. H. Hendon, 2000: Empirical prediction of the Madden–Julian oscillation. *Mon. Wea. Rev.,* **128,** 2528–2543, doi:10.1175/1520-0493(2000)128<2528:EERPOT>2.0.CO;2.

Lorenz, E. N., 1982: Atmospheric predictability experiments with a large numerical model. *Tellus,* **34,** 505–513, doi:10.1111/j.2153-3490.1982.tb01839.x.

Madden, R. A., and P. R. Julian, 1971: Detection of a 40–50 day oscillation in the zonal wind in the tropical Pacific. *J. Atmos. Sci.,* **28,** 702–708, doi:10.1175/1520-0469(1971)028<0702:DOADOI>2.0.CO;2.

Maloney, E. D., and D. L. Hartmann, 2000a: Modulation of hurricane activity in the Gulf of Mexico by the Madden-Julian oscillation. *Science,* **287,** 2002–2004, doi:10.1126/science.287.5460.2002.

——, and ——, 2000b: Modulation of eastern North Pacific hurricanes by the Madden–Julian oscillation. *J. Climate,* **13,** 1451–1460, doi:10.1175/1520-0442(2000)013<1451:MOENPH>2.0.CO;2.

——, and ——, 2001: The sensitivity of intraseasonal variability in the NCAR CCM3 to changes in convective parameterization. *J. Climate,* **14,** 2015–2034, doi:10.1175/1520-0442(2001)014<2015:TSOIVI>2.0.CO;2.

Matthews, A. J., 2008: Primary and successive events in the Madden-Julian oscillation. *Quart. J. Roy. Meteor. Soc.,* **134,** 439–453, doi:10.1002/qj.224.

Molteni, F., R. Buizza, T. N. Palmer, and T. Petroliagis, 1996: The ECMWF ensemble prediction system: Methodology and validation. *Quart. J. Roy. Meteor. Soc.,* **122,** 73–119, doi:10.1002/qj.49712252905.

Moncrieff, M. W., D. E. Waliser, M. J. Miller, M. A. Shapiro, G. R. Asrar, and J. Caughey, 2012: Multiscale convective organization and the YOTC virtual global field campaign. *Bull. Amer. Meteor. Soc.,* **93,** 1171–1187, doi:10.1175/BAMS-D-11-00233.1.

Murphy, A. H., 1973: A new vector partition of the probability score. *J. Appl. Meteor.,* **12,** 595–600, doi:10.1175/1520-0450(1973)012<0595:ANVPOT>2.0.CO;2.

Pegion, K., and B. Kirtman, 2008a: The impact of air–sea interactions on the predictability of the tropical intraseasonal oscillation. *J. Climate,* **21,** 5870–5886, doi:10.1175/2008JCLI2209.1.

——, and ——, 2008b: The impact of air–sea interactions on the simulation of tropical intraseasonal variability. *J. Climate,* **21,** 6616–6635, doi:10.1175/2008JCLI2180.1.

Rashid, H. A., H. H. Hendon, M. C. Wheeler, and O. Alves, 2011: Prediction of the Madden–Julian oscillation with the POAMA dynamical prediction system. *Climate Dyn.,* **36,** 649–661, doi:10.1007/s00382-010-0754-x.

Reichler, T., and J. O. Roads, 2005: Long-range predictability in the tropics. Part II: 30–60-day variability. *J. Climate,* **18,** 634–650, doi:10.1175/JCLI-3295.1.

Saha, S., and Coauthors, 2006: The NCEP Climate Forecast System. *J. Climate,* **19,** 3483–3517, doi:10.1175/JCLI3812.1.

——, and Coauthors, 2014: The NCEP Climate Forecast System version 2. *J. Climate,* **27,** 2185–2208, doi:10.1175/JCLI-D-12-00823.1.

Scoccimarro, E., and Coauthors, 2011: Effects of tropical cyclones on ocean heat transport in a high resolution coupled general circulation model. *J. Climate,* **24,** 4368–4384, doi:10.1175/2011JCLI4104.1.

Seo, K.-H., J.-K. E. Schemm, C. Jones, and S. Moorthi, 2005: Forecast skill of the tropical intraseasonal oscillation in the NCEP GFS dynamical extended range forecasts. *Climate Dyn.,* **25,** 265–284, doi:10.1007/s00382-005-0035-2.

——, W. Wang, J. Gottschalck, Q. Zhang, J.-K. E. Schemm, W. R. Higgins, and A. Kumar, 2009: Evaluation of MJO forecast skill from several statistical and dynamical forecast models. *J. Climate,* **22,** 2372–2388, doi:10.1175/2008JCLI2421.1.

Slingo, J. M., and Coauthors, 1996: Intraseasonal oscillations in 15 atmospheric general circulation models: Results from an AMIP diagnostic subproject. *Climate Dyn.,* **12,** 325–357, doi:10.1007/BF00231106.

Sperber, K. R., and D. Waliser, 2008: New approaches to understanding, simulating, and forecasting the Madden–Julian oscillation. *Bull. Amer. Meteor. Soc.,* **89,** 1917–1920, doi:10.1175/2008BAMS2700.1.

Straub, K. H., 2013: MJO Initiation in the real-time multivariate MJO index. *J. Climate,* **26,** 1130–1151, doi:10.1175/JCLI-D-12-00074.1.

Toth, Z., and E. Kalnay, 1993: Ensemble forecasting at NMC: The generation of perturbations. *Bull. Amer. Meteor. Soc.,* **74,** 2317–2330, doi:10.1175/1520-0477(1993)074<2317:EFANTG>2.0.CO;2.

——, and ——, 1997: Ensemble forecasting at NCEP and the breeding method. *Mon. Wea. Rev.,* **125,** 3297–3319, doi:10.1175/1520-0493(1997)125<3297:EFANAT>2.0.CO;2.

Vialard, J., F. Vitart, M. A. Balmaseda, T. N. Stockdale, and D. L. T. Anderson, 2005: An ensemble generation method for seasonal forecasting with an ocean–atmosphere coupled model. *Mon. Wea. Rev.,* **133,** 441–453, doi:10.1175/MWR-2863.1.

Vintzileos, A., and H.-L. Pan, 2007: On the importance of horizontal resolution and initial conditions to forecasting tropical intraseasonal oscillations: The Maritime Continent prediction barrier. Extended Abstracts, *NOAA/CTB-COLA Joint Seminar,* Camp Springs, MD, NOAA/CTB and COLA. [Available online at http://www.nws.noaa.gov/ost/climate/STIP/CTB-COLA/Augustin_091907.htm.]

Vitart, F., and F. Molteni, 2010: Simulation of the Madden-Julian oscillation and its teleconnections in the ECMWF forecast system. *Quart. J. Roy. Meteor. Soc.,* **136,** 842–855, doi:10.1002/qj.623.

——, S. Woolnough, M. A. Balmaseda, and A. M. Tompkins, 2007: Monthly forecast of the Madden–Julian oscillation using a coupled GCM. *Mon. Wea. Rev.,* **135,** 2700–2715, doi:10.1175/MWR3415.1.

——, A. W. Robertson, and D. L. T. Anderson, 2012: Subseasonal to Seasonal Prediction Project: Bridging the gap between weather and climate. *WMO Bull.,* **61,** 23–28.

Waliser, D. E., 2006a: Predictability of tropical intraseasonal variability. *Predictability of Weather and Climate,* T. Palmer and R. Hagedorn, Eds., Cambridge University Press, 275–305.

——, 2006b: Intraseasonal variability. *The Asian Monsoon,* B. Wang, Ed., Springer, 203–257.

——, 2011: Predictability and forecasting. *Intraseasonal Variability of the Atmosphere-Ocean Climate System,* W. K. M. Lau and D. E. Waliser, Eds., 2nd ed. Springer, 433–476.

——, K. M. Lau, W. Stern, and C. Jones, 2003: Potential predictability of the Madden–Julian oscillation. *Bull. Amer. Meteor. Soc.,* **84,** 33–50, doi:10.1175/BAMS-84-1-33.

Wheeler, M. C., and K. M. Weickmann, 2001: Real-time monitoring and prediction of modes of coherent synoptic to intraseasonal tropical variability. *Mon. Wea. Rev.,* **129,** 2677–2694, doi:10.1175/1520-0493(2001)129<2677:RTMAPO>2.0.CO;2.

——, and H. H. Hendon, 2004: An all-season real-time multivariate MJO index: Development of an index for monitoring and prediction. *Mon. Wea. Rev.,* **132,** 1917–1932, doi:10.1175/1520-0493(2004)132<1917:AARMMI>2.0.CO;2.

Whitaker, J. S., and A. F. Loughe, 1998: The relationship between ensemble spread and ensemble mean skill. *Mon. Wea. Rev.,* **126,** 3292–3302, doi:10.1175/1520-0493(1998)126<3292:TRBESA>2.0.CO;2.

Woolnough, S. J., F. Vitart, and M. Balmaseda, 2007: The role of the ocean in the Madden–Julian oscillation: Sensitivity of an MJO forecast to ocean coupling. *Quart. J. Roy. Meteor. Soc.,* **133,** 117–128, doi:10.1002/qj.4.

Zhang, C., 2005: Madden-Julian oscillation. *Rev. Geophys.,* **43,** RG2003, doi:10.1029/2004RG000158.

——, and J. Gottschalck, 2002: SST anomalies of ENSO and the Madden–Julian oscillation in the equatorial Pacific. *J. Climate,* **15,** 2429–2445, doi:10.1175/1520-0442(2002)015<2429:SAOEAT>2.0.CO;2.

——, ——, E. D. Maloney, M. Moncrieff, F. Vitart, D. E. Waliser, B. Wang, and M. C. Wheeler, 2013: Cracking the MJO nut. *Geophys. Res. Lett.,* **40,** 1223–1230, doi:10.1002/grl.50244.

Zhang, Q., and H. Van den Dool, 2012: Relative merit of model improvement versus availability of retrospective forecasts: The case of Climate Forecast System MJO prediction. *Wea. Forecasting,* **27,** 1045–1051, doi:10.1175/WAF-D-11-00133.1.

Zheng, Y., D. E. Waliser, W. F. Stern, and C. Jones, 2004: The role of coupled sea surface temperatures in the simulation of the tropical intraseasonal oscillation. *J. Climate,* **17,** 4109–4134, doi:10.1175/JCLI3202.1.